Effect of Copper Addition on Oxide Properties and Corrosion Resistance of Niobium Containing Zirconium Alloy in High Dissolved Hydrogen Primary Water Chemistry

Yunju Lee[a], Taeho Kim[a], and Ji Hyun Kim[a]*
[a] *Department of Nuclear Engineering, School of Mechanical, Aerospace and Nuclear Engineering, Ulsan National Institute of Science and Technology, 50 UNIST-gil, Ulsan 44919*
[*] *Corresponding author: kimjh@unist.ac.kr*

1. Introduction

Zirconium alloys are used for fuel cladding of pressurized water reactor (PWR), because they have a very low thermal neutron capture cross section and acceptable mechanical properties. By previous research, it has been reported that the corrosion of zirconium alloys degrades the mechanical properties, and limit the usage of zirconium alloys as fuel cladding material. Recently, in economic context, burnup extension of nuclear power plant is needed, and the burnup extension cannot be achieved without the enhancement of zirconium alloy corrosion resistance. Therefore, the corrosion mechanism of zirconium alloys should be investigated for the safety and economic improvement of nuclear power plant.

The corrosion mechanism of zirconium alloys is closely related with its oxidation behavior. Zirconium alloys spontaneously oxidized at room temperature in oxygen-containing environment because of its strong affinity for oxygen. And it forms passive oxide layer which can protect metal from chemical and mechanical attack. Thus, it is important to understand the oxide behavior of zirconium alloys.

In many previous research, it has been shown that the high temperature oxidation of zirconium leads to the growth of an oxide scale which consists in a mixture of tetragonal and monoclinic phases. Tetragonal phase zirconium oxide is stable at high temperature above 1150 °C, but it has been known that it can be stabilized at lower temperatures in the presence of high compressive stresses. During oxidation process, the protective tetragonal zirconium oxide layer develops at the interface due to accumulated high stress during oxide growth, and it turns into non-protective monoclinic zirconium oxide with increasing oxide thickness, thus decreasing the stress. By previous studies, it has been known that stabilized tetragonal phase zirconium oxide can be used as indicator of good corrosion resistance.

It has been reported that Nb addition was proven to be very beneficial for increasing the corrosion resistance of the zirconium alloys. From a more recent study, Cu addition in Nb containing Zirconium alloy was reported to be effective for increasing corrosion resistance in water containing B and Li. According to the previous research conducted, Zr-Nb-Cu shows better corrosion resistance than Zircaloy-4.

The dissolved hydrogen (DH) concentration is the key issue of primary water chemistry, and the effect of DH concentration on the corrosion rate of nickel based alloy has been researched. However, the effect of DH on the zirconium alloy corrosion mechanism was not fully investigated.

In this research, the zirconium alloys, Zr-Nb-Cu and Zr-Nb-Sn, are oxidized in high DH concentration, 50 cc/kg for 20 days. Then, the transmission electron microscopy (TEM) is used to investigate the oxide growth of zirconium-water interface. The chemical composition of the specimens is also analyzed through energy-dispersive X-ray spectroscopy (EDS). The ex-situ Raman spectroscopic measurement is performed to investigate monoclinic phase zirconium oxide and tetragonal phase zirconium oxide. And the effect of the different chemical composition on the zirconium oxide and the corrosion rate is studied.

2. Experimental

2.1. Specimen preparation

Two different types of zirconium alloys, Zr-Nb-Cu and Zr-Nb-Sn alloy plates were used for this research replicating the primary system of pressurized water reactor. The chemical compositions of two specimens are presented in Table 1. The specimen size of Zr-Nb-Sn is 10 mm × 10 mm × 0.6 mm, and the specimen size for Zr-Nb-Cu is 10 mm × 10 mm × 0.75 mm, and they are polished before oxidization process. First, the SiC paper is used for grinding from 400 grit to 800 grit. Then, the polishing is conducted using 1 μm diamond paste. Finally, to minimize the mechanical transformation to zirconium alloy specimens, the 0.05 μm colloidal silica is used for polishing.

2.2 Procedure for corrosion experiment in simulated PWR water conditions

For this experiment, the polished Zr-Nb-Cu and Zr-Nb-Sn alloy plates were prepared. To simulate high temperature and high pressure the loop system with autoclave is utilized [1]. Using this simulating system, the primary water chemistry of PWR is set, temperature is 360 °C, pressure is 19 MPa, dissolved oxygen concentration is under 10 ppb, LiOH and H_3BO_3 concentration is 2 and 1200 ppm each. In this experiment, the two zirconium alloy plate specimens are oxidized in primary water chemistry for 20 days, and the DH concentration is maintained 50 cc/kg.

To characterize the microscale properties of oxide, the ex-situ investigation was conducted using JEOL JEM-2100F TEM in coincidence with EDS. The

Table. 1 Chemical composition of Zr-Nb-Sn and Zr-Nb-Cu (in wt.%)

Alloy	Nb	Sn	Hf	Cu	C	O	N	Fe	Zr
Zr-Nb-Sn	0.96	0.76	0.002	-	0.1	0.62	0.03	0.18	Bal.
Zr-Nb-Cu	0.55	0.06	-	0.12	0.01	-	-	0.07	Bal.

TEM samples are prepared by focused ion beam(FIB) milling method with a Quanta 3D Dual-Beam Focused Ion Beam (FIB) attached to a field-emission gun scanning electron microscope (SEM). And to investigate the monoclinic phase zirconium oxide and tetragonal phase zirconium oxide in the oxide of the zirconium alloys ex-situ Raman spectroscopic measurement was performed on the surface of the specimens using Alpha300R with 532nm wavelength ND:YAG laser in 10mW power. And the laser penetration depth is considered to be ~1μm.

3. Results and Discussion

3.1 TEM analysis

The oxide properties of Zr-Nb-Sn alloy and Zr-Nb-Cu alloy in 360 °C of high dissolved hydrogen primary water for 20 days were characterized by TEM analysis. The scanning TEM images of (a) Zr-Nb-Cu alloy oxide and (b) Zr-Nb-Sn alloy oxide are shown in Fig. 1. From these images, the oxide thickness of each specimen are measured 10 times in equidistant interval, then average oxide thickness and standard deviation are appeared in Table. 2. The average oxide thickness of Zr-Nb-Sn alloy is thicker than that of Zr-Nb-Cu alloy, which means that the corrosion resistance of Cu-containing zirconium alloy is better than that of Sn-containing zirconium alloy. These results are well matched with previous studies [2,3] conducted for Zr-Nb-Cu alloy.

From Fig. 1, the difference of precipitates distribution between two specimens could be found. Zr-Nb-Cu alloy has larger number of smaller precipitates than Zr-Nb-Sn alloy. The result of point EDS analysis which is conducted for the bulk oxide and the precipitates is appeared in Table. 3, which shows that the precipitates are Nb-containing precipitate. To characterized the structure of the niobium precipitates, fast Fourier transform method was employed for analyzing the diffraction pattern from high-resolution TEM image in Fig. 2. The precipitate is identified to tetragonal phase NbO_2. Thus, it can be resulted to that the Zr-Nb-Cu alloy has larger number of smaller niobium precipitates in its oxide than Zr-Nb-Sn alloy. These results coincident with previous researches that conducted for copper and niobium containing zirconium alloys[3,4], which show that copper addition increases the number of relatively smaller niobium precipitates in Nb-containing zirconium alloy.

Table. 2 Measured oxide thickness from TEM image of two zirconium alloy specimens

Alloy	Average oxide thickness [μm]	Standard deviation
Zr-Nb-Cu	1.30	0.073
Zr-Nb-Sn	1.45	0.063

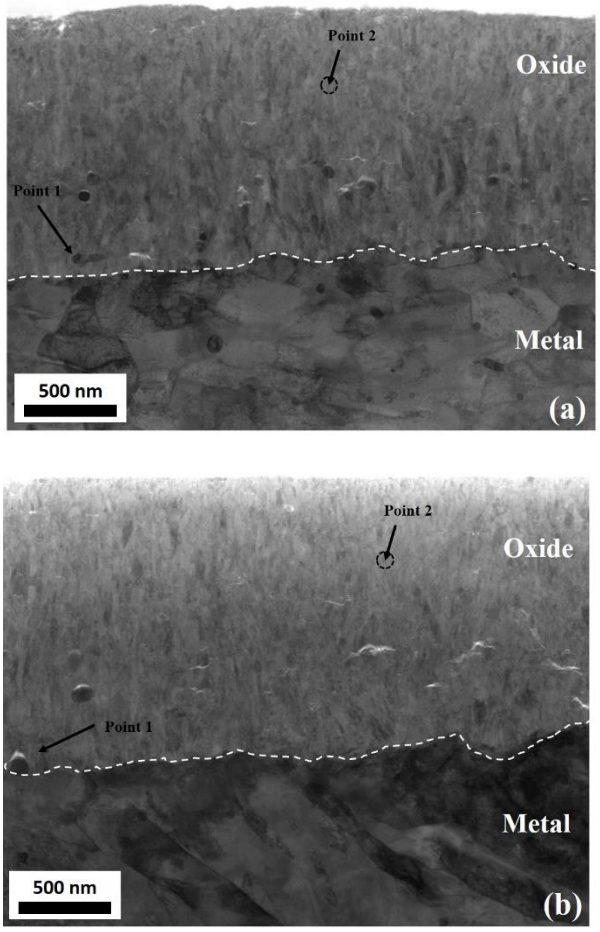

Fig. 1 STEM image of oxidized zirconium alloys in primary water chemistry. (a) Zr-Nb-Cu alloy and (b)Zr-Nb-Sn alloy

Table. 3 Point EDS results of the zirconium alloys in at.%

	Zr-Nb-Cu alloy		Zr-Nb-Sn alloy	
	Point 1	Point 2	Point 1	Point 2
	Precipitate	Bulk	Precipitate	Bulk
O	49.79	60.65	31.40	58.28
Cu	0.092	0.093	-	-
Zr	32.03	38.52	23.26	39.61
Nb	17.33	0.021	43.9274	0.523
Sn	0.741	0.709	1.406	1.576

From these results, the relationship between the copper concentration in Nb-containing zirconium alloy and its good corrosion resistance can be established. According to the previous study, the distribution of niobium precipitates highly affect the distribution of compressive stress of the zirconium alloy oxide [2,3,5]. In Nb containing zirconium alloy, the fine niobium precipitates which are located in the oxide/metal

interface can distribute compressive stress [3,5]. And it delays release of compressive stress so that compressive stress could be distributed in larger oxide/metal interface region [1,5,6]. Thus it is expected to that the more niobium precipitates are distributed, the more tetragonal phase zirconium oxide exist [3], which means that the corrosion resistance of the zirconium alloy is better [1,3,5,6].

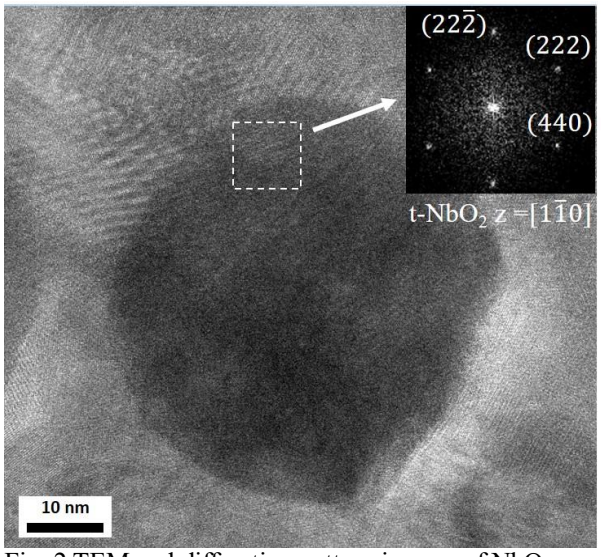

Fig. 2 TEM and diffraction pattern images of NbO_2 precipitate in Zr-Nb-Cu alloy.

3.3 Raman spectroscopy

As explained above, tetragonal phase zirconium oxide becomes stable when compressive stress exists. And distribution of compressive stress is highly affected by distribution of precipitates. From the results of TEM analysis, the small niobium precipitates appear to exist more densely in Zr-Nb-Cu alloy than Zr-Nb-Sn alloy. Thus, it is expected that Zr-Nb-Cu alloy oxide could have more tetragonal phase zirconium oxide than Zr-Nb-Sn alloy oxide. Ex situ Raman spectroscopic measurement was conducted on the two specimens. Fig. 3 shows that the measured Raman spectrum results of the two zirconium alloys. The Raman spectrum intensity of two specimens is normalized and the monoclinic phase zirconium oxide peak (M) and tetragonal phase zirconium oxide peak (T) is marked following previous research [5]. And the detail specification of Raman peak obtained from the two specimens is shown in Table. 4. The peaks located at 177, 224, 308, 380, 474, 503, 616, 639 cm^{-1} show monoclinic phase zirconium oxide of Zr-Nb-Cu alloy oxide and the peaks located at 279, 331, 439 cm^{-1} show tetragonal phase zirconium oxide of Zr-Nb-Cu alloy oxide. The peaks shown at 179, 223, 306, 383, 479, 503, 616, 639 cm^{-1} are attribute to monoclinic phase zirconium oxide of Zr-Nb-Sn alloy oxide and the peaks positioned at 280, 335, 562 cm^{-1} show tetragonal phase zirconium oxide of Zr-Nb-Sn alloy oxide.

Two peaks located at 279 cm^{-1} and 562 cm^{-1} of Zr-Nb-Cu alloy, which appear tetragonal phase zirconium oxide, have stronger intensity than that of Zr-Nb-Sn alloy. And as shown in Fig. 3, more tetragonal phase Raman peak position appears in spectrum of Zr-Nb-Cu alloy oxide than Zr-Nb-Sn alloy oxide, like 439 cm^{-1} peak position.

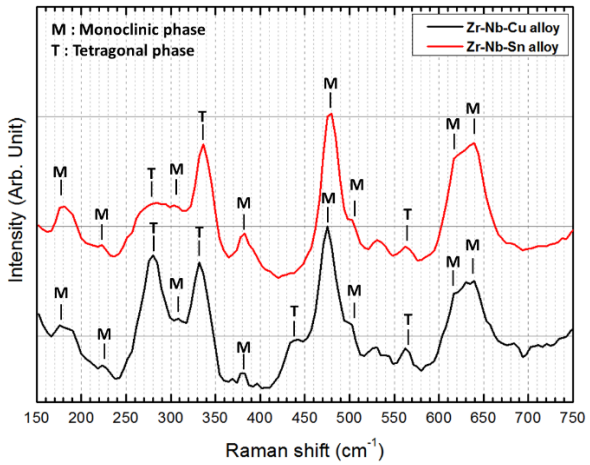

Fig. 3 Measured Raman spectrum of Zr-Nb-Cu alloy and Zr-Nb-Sn alloy oxide excited by a laser at 532 nm at room temperature in air.

Table. 4 Specification of Raman peak position obtained from the two specimens

Zr-Nb-Cu		Zr-Nb-Sn	
Monoclinic	Tetragonal	Monoclinic	Tetragonal
177		179	
224	279	223	279
308	331	306	335
380		383	
474	439	479	
503		503	
616	562	616	562
639		639	

From above Raman spectrum, it is possible to calculate a percentage of tetragonal phase zirconium according to Garvie-Nicholason equation[5,6].

$$\%\ \mathbf{ZrO_{2(T)}} = \frac{\sum Intensity_{(T)}}{\sum Intensity_{(T)} + \sum Intensity_{(M)}} \quad (1)$$

Table. 5 Calculated percentage of tetragonal phase zirconium oxide.

Alloy	Zr-Nb-Cu	Zr-Nb-Sn
% Tetragonal zirconium oxide	41.2	13.8

For calculating the summation of the tetragonal intensity 279, 333, 439 cm^{-1} were chosen and for calculation the summation of the monoclinic intensity 178, 474, 616, 639 cm^{-1} were chosen and calculated tetragonal phase zirconium intensity is shown in Table 5. The 178 and 333 cm^{-1} peaks represent the Zr-Zr vibration mode, and the 474 and 616 cm^{-1} peaks can be attributed to the O-O vibration mode [1,5].

As shown in Table. 5, the percentage of tetragonal phase zirconium oxide in Zr-Nb-Cu alloy oxide is larger than that of Zr-Nb-Sn alloy oxide. These result are well matched with the expectation that Zr-Nb-Cu alloy has better corrosion resistance than Zr-Nb-Sn alloy, so that Zr-Nb-Cu alloy has more peak or has stronger intensity tetragonal zirconium oxide peak than Zr-Nb-Sn alloy.

It has been reported that the tetragonal zirconium oxide phase is positioned near the oxide/metal interface and it could act as a barrier layer for oxidizing the zirconium alloy matrix [1,5–7]. The stabilization of the tetragonal zirconium oxide can be explained by the high concentration of alloying elements like Cu and Nb [2,3], the small grain size and the stresses created by the delayed volume expansion of the precipitate compared to the oxide matrix. The Raman spectroscopy results confirms that the tetragonal zirconium oxide fraction is much higher in Zr-Nb-Cu alloy than Zr-Nb-Sn alloy. Due to the alloying elements in Zr-Nb-Cu alloy, the corrosion rate of Zr-Nb-Cu alloy can be slower than it of Zr-Nb-Sn alloy.

4. Conclusion

In this study, HR-TEM analysis, and Raman spectroscopic measurement were conducted to investigate the effects of dissolved hydrogen concentration and the chemical composition on the corrosion resistance and oxide phase of Zr-Nb-Cu alloy and Zr-Nb-Sn alloy after oxidizing in a primary water environment for 20 d. The corrosion rate of Zr-Nb-Cu alloy is slow, when it is compared to Zr-Nb-Sn alloy.

In TEM images, the oxide thickness of Zr-Nb-Cu alloy is measured to be around 1.30 μm and it of Zr-Nb-Sn alloy is measured to be 1.45 μm. Also, the tetragonal phase niobium precipitates are distributed more densely in Zr-Nb-Cu alloy than Zr-Nb-Sn alloy. This phenomenon can be elucidated with the difference in compressive stress in zirconium oxide due to the distribution of niobium precipitates. And according to ex situ Raman spectra, Zr-Nb-Cu alloy oxide has more tetragonal zirconium oxide fraction than Zr-Nb-Sn alloy oxide. Tetragonal zirconium oxide is stabilized with compressive stress. Tetragonal phase exists near oxide/metal interface and as the distance from oxide/metal interface increases, monoclinic phase becomes dominant, because compressive stress exists near oxide/metal interface and released as the distance from oxide/metal interface increase.

ACKNOWLEDGEMENT

This work was financially supported by the International Collaborative Energy Technology R&D Program (No. 20168540000030) of the Korea Institute of Energy Technology Evaluation and Planning (KETEP) which is funded by the Ministry of Trade Industry and Energy, and the National Nuclear R&D program funded by Ministry of Science, ICT and Future Planning, and by the National Nuclear R&D program (NRF-2016M2B2A9A02944861) organized by the National Research Foundation (NRF) of South Korea in support of the Ministry of Science, ICT and Future Planning.

REFERENCES

[1] T. Kim, J. Kim, K.J. Choi, S.C. Yoo, S. Kim, J.H. Kim, Phase Transformation of Oxide Film in Zirconium Alloy in High Temperature Hydrogenated Water, Corros. Sci. 99 (2015) 134–144.

[2] J.Y. Park, B.K. Choi, Y.H. Jeong, Y.H. Jung, Corrosion behavior of Zr alloys with a high Nb content, J. Nucl. Mater. 340 (2005) 237–246.

[3] J.-Y. Park, B.-K. Choi, S.J. Yoo, Y.H. Jeong, Corrosion behavior and oxide properties of Zr–1.1wt%Nb–0.05wt%Cu alloy, J. Nucl. Mater. 359 (2006) 59–68.

[4] Q. Dong, H. Yu, Z. Yao, F. Long, L. Balogh, M.R. Daymond, Study of microstructure and precipitates of a Zr-2.5Nb-0.5Cu CANDU spacer material, J. Nucl. Mater. 481 (2016) 153–163.

[5] L. Kurpaska, J. Favergeon, L. Lahoche, M. El-Marssi, J.L. Grosseau Poussard, G. Moulin, J.M. Roelandt, Raman spectroscopy analysis of air grown oxide scale developed on pure zirconium substrate, J. Nucl. Mater. 466 (2015) 460–467.

[6] J. Wei, P. Frankel, E. Polatidis, M. Blat, A. Ambard, R.J. Comstock, L. Hallstadius, D. Hudson, G.D.W. Smith, C.R.M. Grovenor, M. Klaus, R.A. Cottis, S. Lyon, M. Preuss, The effect of Sn on autoclave corrosion performance and corrosion mechanisms in Zr-Sn-Nb alloys, Acta Mater. 61 (2013) 4200–4214.

[7] A. Yilmazbayhan, E. Breval, A.T. Motta, R.J. Comstock, Transmission electron microscopy examination of oxide layers formed on Zr alloys, J. Nucl. Mater. 349 (2006) 265–281.